AGU PUBLICATIONS

JGR

Journal of Geophysical Research: Space Physics

RESEARCH ARTICLE

10.1002/2013JA019257

Key Points:
- Quantitative investigation of the IMF on the twisting of the magnetotail
- The current sheet has similar twisting behavior to IMF conditions
- The twisting angle from simulations agrees with observations

Correspondence to:
J. Y. Wang,
jywang@spaceweather.ac.cn

Citation:
Wang, J. Y., C. Wang, Z. H. Huang, and T. R. Sun (2014), Effects of the interplanetary magnetic field on the twisting of the magnetotail: Global MHD results, *J. Geophys. Res. Space Physics*, *119*, 1887–1897, doi:10.1002/2013JA019257.

Received 26 JUL 2013
Accepted 26 FEB 2014
Accepted article online 3 MAR 2014
Published online 24 MAR 2014

Effects of the interplanetary magnetic field on the twisting of the magnetotail: Global MHD results

J. Y. Wang[1,2], C. Wang[1], Z. H. Huang[1], and T. R. Sun[1]

[1]State Key Laboratory of Space Weather, Center for Space Science and Applied Research, Chinese Academy of Sciences, Beijing, China, [2]College of Earth Science, University of Chinese Academy of Sciences, Beijing, China

Abstract We used the global magnetohydrodynamic (MHD) simulation to investigate effects of the interplanetary magnetic field (IMF) on the twisting of the magnetotail. It is shown that the cross section of the magnetotail is elongated along a certain direction close to the IMF orientation. The elongated direction twists with the IMF orientation, magnitude, and the distance away from Earth, and the quantitative relationship has been given. In addition, the current sheet has a similar twisting behavior as the magnetotail magnetopause, with a smaller twisting angle. Our simulated results fall within the range that people have deduced from observations.

1. Introduction

Geomagnetic field lines that are stretched due to reconnection with interplanetary magnetic field (IMF) form the geomagnetic tail on the nightside of Earth; therefore, the structure and shape of the magnetotail are strongly affected by the IMF. The north-south component (B_z) of the IMF is the main factor to determine magnetic reconnections; however, the dawn-dusk component (B_y) of IMF influences the large-scale configuration of the magnetotail as well. It was shown that the existence of IMF B_y could lead to a dawn-dusk bending of tail field lines and a twisting of the entire tail [*Cowley*, 1981].

The characteristic of the magnetotail and its response to the IMF were studied using IMP-8, ISEE-3, and Geotail data in different distances of magnetotail. The bending of tail field lines is connected to the existence of additional IMF B_y field in the entire tail. From numerous observations, the results of the IMF B_y penetration field are nonuniform. The average B_y penetration in the tail accounts for around 10 to 14% of the total IMF B_y magnitude [e.g., *Fairfield*, 1979; *Cowley*, 1981; *Kaymaz et al.*, 1994]. Many statistical studies showed that in the presence of IMF B_y, the current sheet has a twisting of about 6 to 18° away from the equatorial plane [e.g., *Sibeck et al.*, 1986; *Tsyganenko et al.*, 1998; *Kaymaz et al.*, 1994]. Using observations of the Pioneer 7, *Villante* [1976] found that magnetotail at −200 R_E can twist up to 20°. From the observations of ISEE-3, *Sibeck et al.* [1986] obtained the average angle of current sheet twisting about 18°. *Owen et al.* [1995] analyzed vast current sheet twisting cases which were obtained from the near tail to the distant tail (down to 240 R_E) and found that the degree of current sheet twisting is related to the sign of IMF B_z. For southward IMF B_z, the twisting is −12° for $B_y > 0$ and 6° for $B_y < 0$, and for northward IMF B_z, it is −24° for $B_y > 0$ and 13° for $B_y < 0$.

MHD numerical simulations were used to investigate the effect of IMF B_y on the magnetotail. *Brecht et al.* [1981] executed a run with a solar wind which has a B_y magnetic component besides a B_z component input. The results showed an IMF B_y penetration into the tail and a twisting of the entire tail. *Kaymaz et al.* [1995] studied the cross-sectional magnetic field configuration and the twisting of current sheet by the Fedder-Lyon MHD model [*Lyon et al.*, 2004]. It was shown that both the IMF B_y penetration and twisting of current sheet agree with the results from previous observations [*Kaymaz et al.*, 1994]. In addition, several work presented MHD simulated results for a changing IMF clock angle. *Berchem et al.* [1998] compared the simulated results with Geotail observed data of the tail during a period of changing IMF. They found that the response of the distant tail is driven by the changing clock angle of IMF; the closed field line region is long and the plasma sheet twists violently for small IMF clock angles only. A more detailed study for a changing IMF clock angle is provided by *Walker et al.* [1999] using MHD simulations. The simulated results showed that the near-Earth tail responds first to an IMF change but twists more slightly than the distant tail. The tail alters its twisting first at the flanks, then in the central tail with the changing IMF clock angle.

The deformation of magnetotail configuration is often described by the cross-sectional shape of the magnetotail. Early satellite observations of the near-Earth magnetotail displayed that the cross section of tail is

a circle or slightly elongated in the GSM *z* direction [*Behannon*, 1968, 1970; *Fairfield*, 1971; *Scarf et al.*, 1977]. Most empirical magnetopause models [e.g., *Sibeck et al.*, 1991; *Petrinec and Russell*, 1996; *Shue et al.*, 1997; *Kawano et al.*, 1999] also adopted the hypothesis that magnetopause is rotational symmetric about the aberrated Sun-Earth line and has a rounded section at magnetotail. *Lu et al.* [2011] developed a numerical three-dimensional magnetopause model considering the impact of IMF B_z and solar wind dynamic pressure (D_p) on the shape of magnetopause. They showed that the dayside magnetopause shape in the *yz* plane is an oval elongated along the *y* direction, and the magnetotail magnetopause is an oval elongated along the *z* direction. Using the theoretical analysis and MHD simulations, *Lavraud and Borovsky* [2008] suggested that, in addition to accelerating flows tailward along the magnetopause, enhanced magnetic forces in the magnetosheath during strong IMF exert an asymmetric pressure on the magnetopause so that it may deform and get elongated in the direction of IMF. Previous work also specially investigated the situations of distant geomagnetic tail. *Berchem et al.* [1998] showed that the cross section of the distant tail was considerably flattened along the direction perpendicular to the IMF clock angle. *Hasegawa et al.* [2002a, 2002b] studied IMF dependence of the distant tail shape using the plasma and magnetic field measurement and found that the *yz* cross section of magnetotail stretches along IMF direction. Recently, using the MHD simulations, *Lu et al.* [2013] improved the three-dimensional model on the basis of *Liu et al.* [2012] to investigate the influence of IMF B_y and B_z on the shape of magnetopause. They found that the stretch direction of the magnetopause cross section is always near the direction of the IMF but is a little closer to the meridional plane than the IMF.

Nevertheless, the twisting of the magnetotail at various distances and its quantitative association with the IMF conditions have not been investigated in a systematic way. In this study, we will take advantage of global MHD simulations to study the effect of IMF on the twisting of the magnetotail and try to compare with observations. Section 2 will introduce the methodology including the MHD model and the diagnosis methods to determine the magnetopause and the current sheet locations. Section 3 will present the numerical simulated results, and section 4 gives the discussions and summary.

2. Methodology

2.1. The Global Piecewise Parabolic Method With a Lagrangian Remap-MHD Model

The piecewise parabolic method scheme of *Colella and Woodward* [1984] is a high-order extension of the Godunov algorithm [*Godunov*, 1959]. *Hu et al.* [2005, 2007] developed a piecewise parabolic method with a Lagrangian remap (PPMLR)-MHD algorithm for global simulations of solar wind-magnetosphere-ionosphere system. It is an extension of the Lagrangian version of the piecewise parabolic method developed by *Colella and Woodward* [1984] to MHD.

In the algorithm of PPMLR-MHD, all MHD-dependent physical conservative variables are defined at the zone centers as volume averages, and their spatial distributions are obtained by interpolation which is piecewise continuous, with a parabolic profile in each zone. MHD equations in the solar wind-magnetosphere region are cast into a conservation form in Lagrangian coordinates. The algorithm involves three steps:

1. A characteristic method similar to that proposed by *Dai and Woodward* [1995] is used to solve the Riemann problem at the zone edges and obtain the local values of the dependent variables at the halftime point $t^{n+1/2}$. The values are further used to calculate the corresponding effective fluxes.
2. Using the obtained fluxes and starting from the difference approximation of the Lagrangian conservation laws, we update all dependent variables from t_n to t_{n+1} and calculate the new dependent variables in the Lagrangian coordinates.
3. The results are remapped back onto the fixed Eulerian grid through solving the corresponding advection equations.

PPMLR-MHD has high-order spatial accuracy and low numerical dissipation, and it can capture a shock within two numerical zones without any appreciable overshot and undershot. The model uses a Cartesian coordinate system with the Earth center at the origin and the *x*, *y*, and *z* axes pointing to the Sun, the dawn-dusk direction, and the north, respectively. The system is assumed to be symmetrical about the equatorial planes and noon-midnight meridian, and the solution domain is $-300\ R_E < x < 30\ R_E$, $-150\ R_E < y, z < 150\ R_E$. Inside $-10\ R_E < x < 10\ R_E$, $-10\ R_E < y, z < 10\ R_E$, the grid size is $0.4\ R_E$, and the grid size outside this region increases along each axis with a geometrical series of common ratio 1.05. The total number of grid points is $160 \times 162 \times 162$. A sphere at $3\ R_E$ is set to the inner boundary of magnetosphere in order to avoid the complexity associated with the plasmasphere and strong magnetic

field near the Earth. A magnetospheric-ionospheric electrostatic coupling model is imbedded to drive the inner magnetospheric convection. The ionosphere is set as a spherical surface (R_{ion} = 1.017 R_E) with uniform height-integrated conductance. The field-aligned currents near the inner boundary are mapped into the ionosphere along magnetic field lines. A two-dimensional Poisson equation is used to obtain the electric potential and further calculate the corresponding electric field. Then, the electric field is remapped to the inner boundary to calculate the convective velocity, which is used as the inner boundary condition for the simulation.

For simplicity, all numerical runs are conducted under the following assumptions: (1) the solar wind velocity is along the Sun-Earth line, and the Earth's dipole moment is due southward; (2) the solar wind velocity and number density are fixed to be 400 km s^{-1} and 5 cm^{-3}, and the ionosphere is uniform with a Pedersen conductance $\sum_p$ = 5 *S* and a zero Hall conductance; and (3) the IMF is perpendicular to the Sun-Earth line with a negative *z* component ($B_z < 0$), adjustable strength B_{IMF} and clock angle θ_{CA}: B_{IMF} = 5, 8, 10, 12, 15, 20 nT; θ_{CA} = 100°–260° (an interval of 10°). Each run needs to continue for more than 5 h in physical time until the solar wind-magnetosphere-ionosphere system reaches a quasi steady state.

2.2. Diagnosis Method for the Magnetopause Location

In order to investigate the effects of the IMF on the twisting of the magnetotail, it is important to identify the magnetopause location from the simulations. Generally speaking, there exist several different criterions for the identification of magnetopause location, e.g., the density gradient maximum, current density maximum, and pressure gradient maximum. *Němeček et al.* [2011] presented a method that detects magnetopause based on searching for the peaks of current density and maxima of velocity and number density gradients in global simulated results. However, this method is able to identify the magnetopause boundary to $x = -15\ R_E$ downtail only. By finding approximately the solar wind streamlines encompassing the inner edge of the void, *Palmroth et al.* [2003] developed an automated technique for identifying the magnetopause surface from the simulations. Recently, *Liu et al.* [2012] indicated that the streamline method is not able to determine the subsolar point very well, and they used the peaks of the current density to identify the subsolar magnetopause instead. In this study, we make a slight modification of the streamline method as *Liu et al.* [2012] did.

The procedure of the improved streamline method is described as follows:

1. In GSM coordinate, scan along the positive *x* direction from $x = 6\ R_E$ to $x = 20\ R_E$ and locate the two points which have the first or second largest peak of current density. The one near the Earth is determined as the subsolar point.
2. Create a set of streamline at $x = 20\ R_E$ in the upstream of the bow shock. At first, the streamline grid is defined in *yz* plane in a circle with 20 R_E as its radius and the *x* axis at its center. The distance between the neighboring streamlines is $\Delta R = 0.5\ R_E$, $\Delta\phi = 1°$. The total number of streamlines is 14,400. Started from $x = 20\ R_E$, we trace every streamline for each 0.5 R_E step in the $-x$ direction based on the velocity. Specifically, (x_j, y_{ij}, z_{ij}) is the coordinate of the *i*th streamline in $x = x_j$ plane. (vx_{ij}, vy_{ij}, vz_{ij}) is the corresponding velocity at this point. These values are further used to calculate the coordinate of this streamline in $x = x_{(j+1)}$ plane: $x_{(j+1)} = x_j - 0.5$, $y_{i(j+1)} = y_{ij} - 0.5\ \frac{vy_{ij}}{vx_{ij}}$, $z_{i(j+1)} = z_{ij} - 0.5\ \frac{vz_{ij}}{vx_{ij}}$.
3. For each 0.5 R_E step in the $-x$ direction starting from the subsolar, apply the magnetopause identification procedure in x = const planes. The x = const planes are divided equally into 3° sectors with respect to the azimuthal angle. The total number of sectors is 120. Based on the coordinate of streamlines in x = const planes, we can determine in which sector the streamlines locate. In each sector the streamlines are sorted by their distance from the *x* axis. Three closest streamlines that may flow into the magnetosphere are excluded, and the magnetopause is defined to be the arithmetic mean of the radii of the four next closest streamline. Accordingly, the magnetopause location in each sector in each x = const plane can be obtained. The resulting resolution of the magnetopause surface is 0.5 R_E in the *x* direction and 3° in the *yz* plane. In fact, the distribution of streamlines is intensive around the magnetopause. Thus, varying the number of streamlines excluded from evaluation and the number of streamlines used to compute the mean brought only small changes to the magnetopause location.

Figure 1a shows an example of three-dimensional magnetopause determined by the improved streamline method for B_{IMF} = 20 nT and IMF clock angle θ_{CA} = 260°. Figure 1b shows the number density contour and the detected magnetopause (red line) in different planes. The detected magnetopause is in good agreement with the location on the peak of number density gradient, which validates the streamline method.

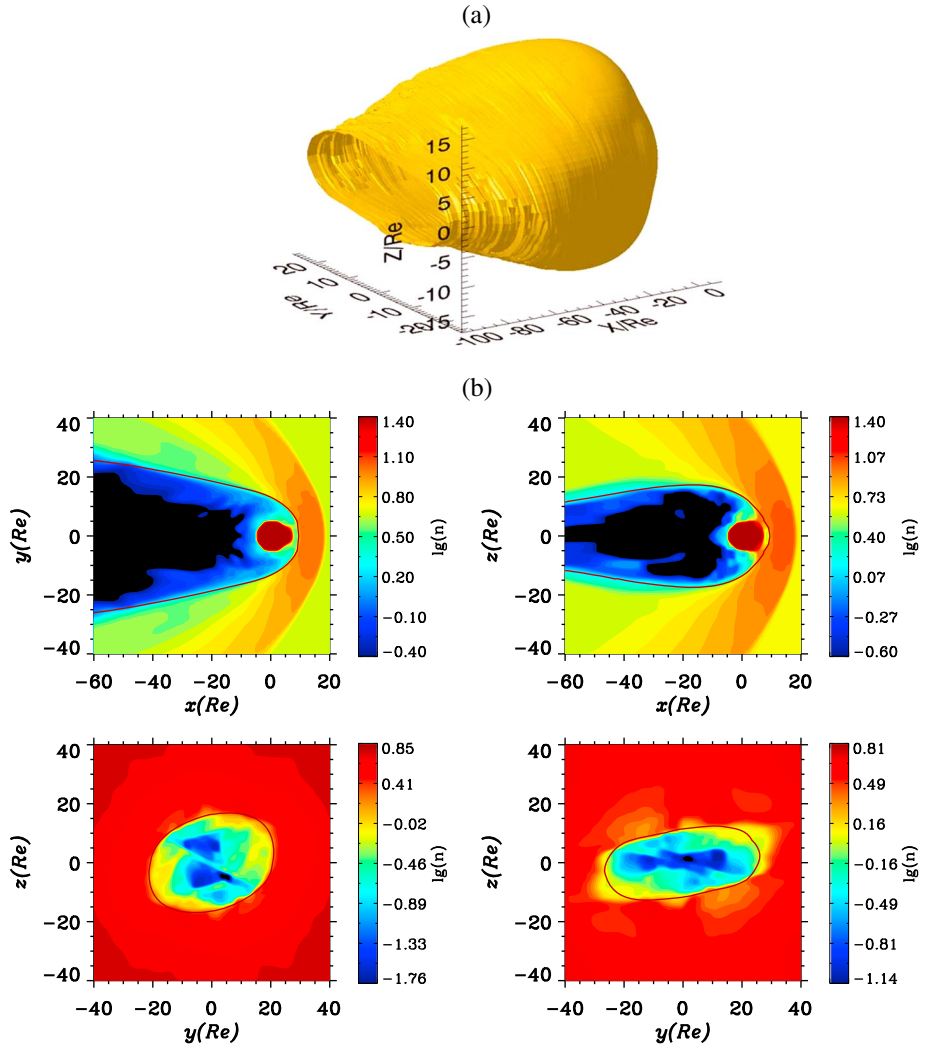

Figure 1. (a) An example of three-dimensional magnetopause determined by improved streamline method for B_{IMF} = 20 nT and IMF clock angle θ_{CA} = 260°. (b) The number density contour and the detected magnetopause (red line) in different planes ((top left) *xoy*, (top right) *xoz*, (bottom left) the *yz* cross section of magnetotail at $x = -30\ R_E$, and (bottom right) the *yz* cross section of magnetotail at $x = -60\ R_E$).

2.3. Diagnosis Method for the Current Sheet Location

For studying the changing relationship between the twisting of current sheet at $x = -20\ R_E$ as an example and the IMF quantitatively, we need to determine the location and twisting angle of the current sheet. Figure 2b illustrates the current density $\left(\sqrt{J_y^2 + J_z^2}\right)$ contour in *yz* section of magnetotail at $x = -20\ R_E$ for B_{IMF} = 20 nT and θ_{CA} = 260°; the location of the current sheet is indicated by the peak of the current density. Hence, we adopt the following procedure to determine the location and thus the twisting angle of current sheet:

1. In the GSM coordinates, discretize the *yz* cross section at $x = -20\ R_E$ into a uniform mesh in the domain of $-14\ R_E \le y \le 14\ R_E$ and $-14\ R_E \le z \le 14\ R_E$, with the spatial difference of $\Delta y = 0.4\ R_E$ and $\Delta z = 0.4\ R_E$.
2. For a given set of grid coordinates y_i, scan along the positive *z* direction from $z = -14\ R_E$ and locate the point z_i, at which is a greatest sharp peak of current density $\sqrt{J_y^2 + J_z^2}$. Figure 2a is an example in which the current density changing along the *z* axis at $x = -20\ R_E$, $y = -12\ R_E$ of the magnetotail.
3. Make the linear fit to the determined points (y_i, z_i), the slope *k* can then be used to describe the twisting of current sheet. The value of twisting angle is $|\arctan(k)|$. As shown in Figure 2b, the red line marks the location of the current sheet.

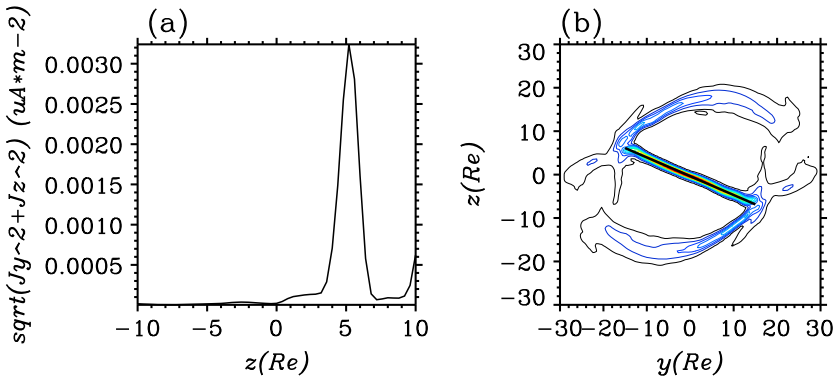

Figure 2. Under the IMF condition B_{IMF} = 20 nT, θ_{CA} = 260°, (a) the changing tendency of current density along the direction of z axis at $x = -20\ R_E$, $y = -12\ R_E$ of magnetotail, (b) the current density $\left(\sqrt{J_y^2 + J_z^2}\right)$ contour in yz cross section of magnetotail at $x = -20\ R_E$, and the location of current sheet determined by searching the peak of current density (red line).

3. Results

3.1. Influence of the IMF on the Twisting of the Magnetotail

Figure 3 plots the different yz cross sections of magnetotail for various IMF conditions. The red solid line represents the location of magnetopause detected by the improved streamline method. Number density contour is presented for illustrating the appropriateness of magnetopause detected by streamline method. The shape of magnetopause is not generally rotational symmetric but an oval elongated along a certain direction near the IMF direction, which is consistent with the conclusion from *Lu et al.* [2013]. In order to determine the elongated direction quantitatively, we fit the magnetopause in every yz cross section of magnetotail by an elliptic equation

$$r = \sqrt{\frac{a^2 b^2}{a^2 \sin^2(\phi + \Delta\theta) + b^2 \cos^2(\phi + \Delta\theta)}} \tag{1}$$

where $r = \sqrt{(y^2 + z^2)}$ is the radial distance from the x axis, ϕ is the azimuth angle in polar coordinates, b and a are the semimajor axis and semiminor axis of this ellipse, respectively, and the $\Delta\theta$ is the twisting

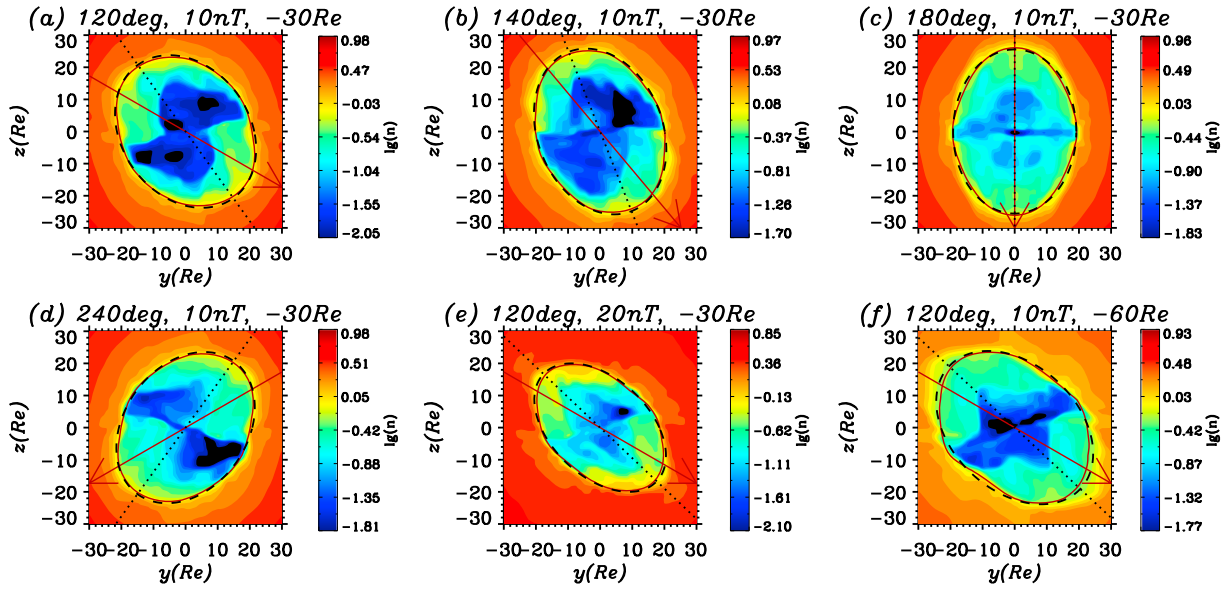

Figure 3. (a–f) Number density contour and magnetopause determined by streamline method (red solid line) and the fitting elliptic equation (black dash line) in different yz cross sections of magnetotail for distinct IMF conditions. In each panel, black dot line stands for the stretched direction of magnetopause; an arrow denotes the IMF orientation.

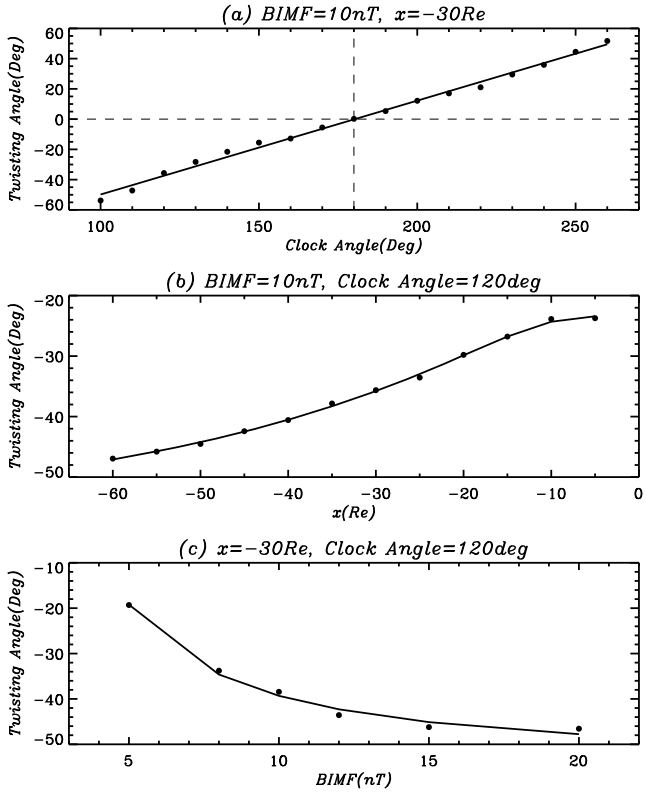

Figure 4. Magnetopause twisting angle θ_{twm} as functions of θ_{CA}, B_{IMF}, and x; the dots are the results calculated from simulations, and three solid lines are determined by equations (2)–(4), respectively. (a) θ_{twm} as functions of θ_{CA}. (b) θ_{twm} as functions of x. (c) θ_{twm} as functions of B_{IMF}.

angle of semimajor axis deviated from z axis. In each panel of Figure 3 appointed for a specific IMF condition and distance from Earth, the black dash line represents the magnetopause shape calculated from the fitting equation, and the black dot line indicates its elongated direction. Since the black dash lines are in good agreement with the magnetopause location detected by the improved streamline method, it is rational to use an ellipse to represent the shape of magnetopause in yz cross section of magnetotail and determine the elongated direction by its semimajor axis. When the IMF direction deviates from due southward (due to the presence of IMF B_y), the elongated direction of the magnetotail magnetopause twists from the south-north direction as well (Figures 3a–3c). The twisting is counterclockwise under a positive y component of the IMF. With decreasing IMF clock angle, the twisting angle increases. There is an angle between the elongated direction of magnetopause and the IMF orientation, which increases with the decreasing IMF clock angle. When the IMF is due southward, the elongated direction of the magnetotail magnetopause is strictly along the IMF orientation. Figure 3d shows the case of $\theta_{CA} = 240°$ in order to make comparison with the case of $\theta_{CA} = 120°$. The two magnetopause contours roughly satisfy mirror symmetry, though they have some subtle differences. We compare Figures 3a with 3e and 3f and find that the twisting of magnetotail magnetopause increases with the increase of the IMF magnitude and the distance from Earth. The twisting of the magnetotail magnetopause seems related to three parameters: the IMF clock angle θ_{CA}, IMF magnitude B_{IMF}, and distance from Earth.

Now we examine quantitatively the change of the twisting with the above mentioned three parameters. The $\Delta\theta$ in elliptic equation (1) can be used to depict the twisting angle of magnetopause in the magnetotail. Viewed from the Sun, the magnetopause twists clockwise if $\Delta\theta$ is positive and counterclockwise if $\Delta\theta$ is negative. We do simulations for the IMF conditions of $B_{IMF} = 5$, 8, 10, 12, 15, and 20 nT and $\theta_{CA} = 100° \sim 260°$ (with an interval of 10°) and fit the shape of magnetopause at $x \geq -60\ R_E$ (as an example) of the magnetotail by equation (1) to determine $\Delta\theta$ or the twisting angle of magnetopause θ_{twm}. In order to discuss the relationship between the twisting angle and one specific parameter, we keep the other two parameters

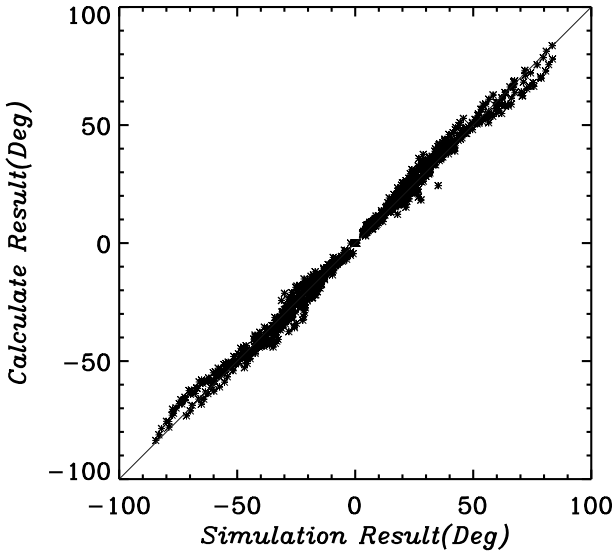

Figure 5. Comparison between the results from simulations and those calculated by equation (6).

unchanged. Figure 4a shows the twisting angle θ_{twm} as a function of the IMF clock angle θ_{CA}. The dots are the simulated results. The fitting relationship is in the form of

$$\theta_{twm} = c_1 \cdot \theta_{CA} + c_2 \tag{2}$$

With the increasing IMF clock angle θ_{CA}, the value of the twisting angle θ_{twm} increases (considering the sign). Figure 4b shows the twisting angle θ_{twm} as a function of the distance x. Similarly, the dots are the simulated results, and the fitting relationship is in the form of

$$\theta_{twm} = c_1 \cdot \exp(c_2/x) + c_3 \tag{3}$$

The absolute value of the twisting angle θ_{twm} increases with the increasing $|x|$. It means that the twisting of magnetotail magnetopause becomes more and more severe with the increasing distance from Earth. Figure 4c illustrates the twisting angle θ_{twm} as a function of the IMF magnitude B_{IMF}. The fitting relationship is in the form of

$$\theta_{twm} = c_1 \cdot B_{IMF}^{c_2} + c_3 \tag{4}$$

A stronger B_{IMF} usually leads to a larger twisting of the magnetotail up to about 20 nT.

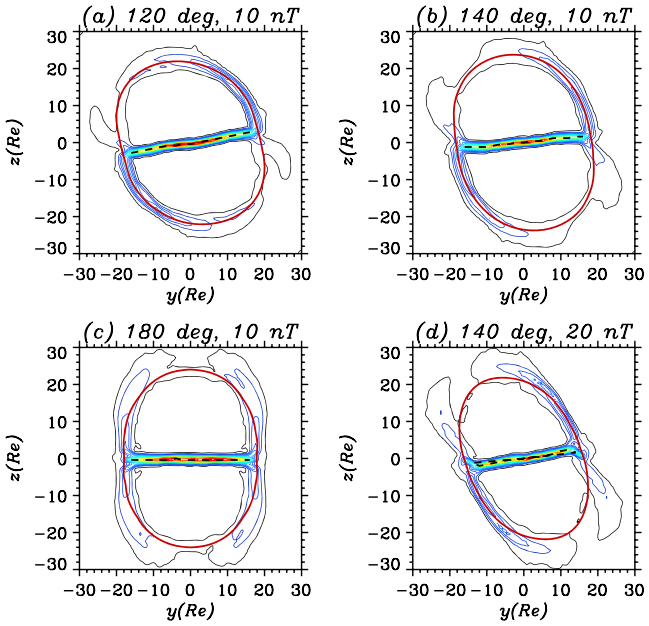

Figure 6. (a–d) Current density $\left(\sqrt{J_y^2 + J_z^2}\right)$ contour, magnetopause determined by streamline method (red solid line), and the location of current sheet determined by searching the peak of current density (black dash line).

Putting all three parameters together and considering of the zero twisting angle under pure southward IMF, we find the twisting angle θ_{twm} can be expressed as

$$\theta_{twm} = (\theta_{CA} - 180.00) \cdot \left[\exp\left(\frac{a_1}{|x|}\right) + B_{IMF}^{a_2} + a_3\right] \tag{5}$$

The a_1, a_2, and a_3 depict the extent of impact of x, IMF magnitude, and clock angle on the twisting angle, respectively. We apply the multiple parameters fitting to the simulated results and find that the best fit parameters are

$$\theta_{twm} = (\theta_{CA} - 180.00) \cdot \left[\exp\left(-\frac{38.45}{|x|}\right) + B_{IMF}^{0.16} - 1.08\right] \tag{6}$$

Table 1. Current Sheet Twisting Angle at $x = -20\ R_E$ of Magnetotail for Different IMF Conditions[a]

Twisting Angle	$\theta_{twc}(°)$			
B_{IMF}(nT)	5	10	15	20
$\theta_{CA} = 100°$	−9.7371	−16.9984	−18.8384	−22.2347
$\theta_{CA} = 120°$	−6.6360	−8.1999	−12.2253	−12.5713
$\theta_{CA} = 140°$	−5.0120	−6.0734	−8.7276	−9.5422
$\theta_{CA} = 160°$	−3.3081	−3.7875	−4.5739	−4.1672
$\theta_{CA} = 180°$	−0.0113	0.0000	0.1123	0.0002
$\theta_{CA} = 200°$	2.2807	4.5032	4.2077	4.5215
$\theta_{CA} = 220°$	5.0703	6.1552	8.0483	10.0331
$\theta_{CA} = 240°$	7.0144	12.4931	13.1160	14.6804
$\theta_{CA} = 260°$	9.6027	16.0529	20.5478	23.6647
Express	$0.12\theta_{CA} - 21.69$	$0.19\theta_{CA} - 33.59$	$0.23\theta_{CA} - 41.20$	$0.26\theta_{CA} - 46.49$
Average	6.0841	9.2830	11.2856	12.6769

[a]If twisting angle is positive, current sheet twists in clockwise direction. Otherwise, it twists in counterclockwise direction.

The correlation coefficient of the fitting is about 0.99, with a standard deviation of 3.08. Figure 5 shows the comparison between the results from simulations and the ones calculated by equation (6). If the simulated result is consistent with the fitting result, the points should locate on the diagonal. The points away from the diagonal would be an indication of the deviation existing between the two results. As shown in Figure 5, the points from the simulations concentrate near the diagonal, which illustrates the fitting function that represents the simulated results quite well.

3.2. Influence of the IMF on the Twisting of the Current Sheet

In this subsection, we discuss the twisting of the current sheet at $x = -20\ R_E$ under different IMF conditions. As shown in Figure 6c when the IMF clock angle $\theta_{CA} = 180°$, the current sheet is in the equatorial plane for due southward IMF. By comparison of Figures 6c and 6a and 6b, when the IMF direction deviates from due southward (due to the presence of IMF B_y), the current sheet twists from the equatorial plane. The direction of the twisting is the same as that of the magnetopause twisting. However, the extent of the twisting is slighter than that of the magnetopause. Similarly, with the decreasing IMF θ_{CA}, the twisting angle increases.

In Figure 6, please note that the magnetopause determined by the maximum of the current density is outside of the streamline position in the low current density region, while they are close to each other in the high current density region. When determining the current density contour, the errors caused by the interpolation has the same order of the current density in the low current density region due to sparse grid points. As a result, the magnetopause as judged by the maximum of the current density does not agree well with the streamline position. Nevertheless, this difference is not significant.

The twisting angle of the current sheet (θ_{twc}) in *yz* cross section of magnetotail at $x = -20\ R_E$ for different IMF conditions are listed in Table 1. The relationship between the twisting angle of the current sheet θ_{twc} and the IMF clock angle θ_{CA} is almost linear. The specific expressions are shown in the penultimate row of Table 1. In addition, for the same IMF clock angle, the current sheet twists more severely resulted from a stronger B_{IMF}, as shown in Figures 6b and 6d.

In the last row of Table 1, we present statistical averages under the assumption that the IMF orientation has an isotropic distribution, except due southward. *Kaymaz et al.* [1994] listed the average twisting angle of current sheet at different average distances of magnetotail as response to the IMF B_y in published literature, which showed that current sheet at near-Earth magnetotail has a twisting of about 6 to 10°. The twisting angle from our simulated results basically fall within this range.

4. Discussions and Summary

Using global MHD simulations, we have studied the effect of the IMF conditions on the twisting of the magnetotail quantitatively. In fact, the solar wind-magnetosphere-ionosphere system is controlled by the interplay between the ionospheric load and the solar wind flow. The solar wind condition and ionospheric conductance are the main factors which can make significant effects on this system, including the changing

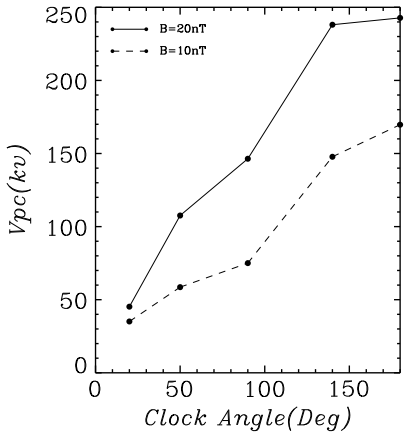

Figure 7. Cross-polar potential versus the IMF clock angle.

of magnetospheric shape, cross-polar potential, etc. Figure 7 is an actual example that illustrates the cross-polar potential as a function of IMF clock angle for B_{IMF} = 10 nT and 20 nT. From *Hu et al.* [2007], the reconnection voltage has significant differences with cross-polar potential; hence, the result in Figure 7 can also be used to assess the strength of ionospheric coupling. In this study, the Pedersen conductance is limited to a constant of 5 Siements which is in the right range for some sort of averaged ionospheric conductance. Thus, it is the solar wind conditions that control the changes of magnetospheric shape and cross-polar potential. We mainly focus on the study about effects of the IMF conditions on the shape of the magnetotail. Further discussions about the relationship between the cross-polar potential (or say, the strength of ionospheric coupling) and magnetospheric shape is beyond the topic of this paper and will be investigated in the future work.

We try to understand the physics lying behind our simulated results. For a southward IMF B_z, the open field lines which originate from the reconnection at dayside magnetopause are dragged toward magnetotail and accumulate over there. Under a due southward IMF, the reconnection occurs near the equator. The magnetic field lines are dragged toward high latitudes of the magnetotail across the northern or southern poles. When the IMF has a dawn-dusk component in addition to the southward B_z, the reconnection sites at dayside magnetopause move to higher latitudes. The convection of open magnetic field lines toward magnetotail has a dawn-dusk component [*Park et al.*, 2006]. For instance, when the IMF has a positive B_y component, the reconnected sites of duskside are at the Northern Hemisphere, and the convection of open field lines caused by reconnection has a dawnward component; while the reconnected sites of dawnside are at the Southern Hemisphere, the convection of open field lines has a duskward component. Figure 8 shows an example which illustrates the accumulated situations of open field lines at $-30\ R_E$ of the magnetotail for $\theta_{CA} = 120°$, B_{IMF} = 10 nT. We set the foot points of the field lines at the inner boundary uniformly and trace these field lines and determine the coordinates of them in space by the Runge-Kutta method. Only the open field lines with a free endpoint are kept. Based on the *y* and *z* coordinates of open field lines at $x = -30\ R_E$, we can obtain the distribution of these lines on this *yz* plane, which are indicated by the color shading in the background. The white arrow denotes the direction of the plasma flow. As seen from Figure 8, open field lines that resulted from reconnection at dayside magnetopause accumulate along the white arrows on the dusk top corner and on the dawn bottom and are resisted by the original magnetic field lines at the magnetotail. As a result, many open field lines gather in the region of warm colors. In the Northern Hemisphere, this region deviates from the meridional plane to dawnside, while in the Southern Hemisphere, it deviates to duskside. Due to the squeezing between the original field lines and the accumulated field lines, part of the open field lines are squeezed and outflow forms as indicated by the white arrows near the diagonal line, which cause the elongation of the magnetopause. As the convection of the newly reconnected open field lines has a dawn-dusk component in the presence of IMF B_y, these field lines deviate from the noon-midnight meridional plane more severely with increasing distance from Earth. As a result, the elongated direction of magnetopause twists larger. *Hu et al.* [2009] indicated that the reconnection sites move to the equator

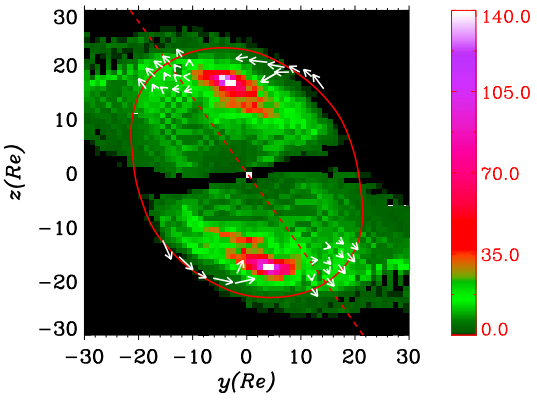

Figure 8. The distribution of open magnetic field lines in $x = -30\ R_E$ cross section of magnetotail for θ_{CA}=120°, B_{IMF} = 10 nT. The red solid line is the location of magnetopause determined by streamline method; the red dash line stands for the elongated direction of magnetopause; and the white arrow denotes the direction of the actual flow in the local, and the length is 0.1 times of flow velocity.

with increasing IMF clock angle. The convection of the open field lines has thus a smaller dawn-dusk velocity for a larger IMF clock angle. Accordingly, for an increased IMF clock angle the elongated direction of magnetopause twists more slightly. In addition, the twisting of the magnetotail increases with enhanced IMF magnitude, mainly resulting from the increased convection velocity of open field lines.

In summary, we analyze the influence of IMF on the twisting of the magnetotail in terms of global PPMLR-MHD simulations. The simulations are limited to cases in which the solar wind velocity is along the Sun-Earth line, the Earth's dipole moment is due southward, and IMF is perpendicular to the Sun-Earth line with a negative z component ($B_z < 0$). We use the improved streamline method to identify the location of the magnetopause in the magnetotail and use the peak of current density $\left(\sqrt{J_y^2 + J_z^2}\right)$ to determine the location of the current sheet. The main results are as follows:

1. The cross sections of the magnetotail are not rotationally symmetric but elongated along a certain direction close to the IMF orientation. The elongated direction twists with the changing IMF magnitude, orientation, and the distance away from Earth. We use an elliptical formula to fit the magnetopause at different distances of magnetotail to determine the twisting angle. With increasing IMF clock angle, the value of twisting angle increases (considering the sign). The twisting of magnetotail magnetopause becomes more severe with the increasing distance away from Earth. The stronger B_{IMF} causes the shape of the entire magnetotail to twist more severely.
2. We find an empirical expression which can describe the relationship between the twisting angle of the magnetopause at different distances of magnetotail and the IMF conditions. The relationship can be expressed in the form of the following:

$$\theta_{\mathrm{twm}} = (\theta_{\mathrm{CA}} - 180.00) \cdot \left[\exp\left(-\frac{38.45}{|x|}\right) + B_{\mathrm{IMF}}^{0.16} - 1.08\right] \tag{7}$$

3. Under different conditions of IMF, the current sheet has a similar twisting behavior with the shape of magnetotail magnetopause, with a smaller twisting angle. Our statistical twisting averages of the current sheet under the assumption that the IMF orientation has an isotropic distribution are very close to the results from observations.

These conclusions are just applicable in the generic southward IMF cases ($B_z < 0$). For the generic northward IMF cases ($B_z > 0$), the magnetotail is also elongated along a certain direction near the IMF orientation but with a slightly smaller twisting angle. Symmetrical study of the effect of the northward IMF component on the magnetotail will be conducted in our future work.

Acknowledgments
This work was supported by the 973 program 2012CB825602, NNSFC grant 41374172, NNSFC grant 41231067, and in part by the Specialized Research Fund for State Key Laboratories of China.

Masaki Fujimoto thanks Zerefsan Kaymaz and an anonymous reviewer for their assistance in evaluating this paper.

References

Behannon, K. (1968), Mapping of the Earth's bow shock and magnetic tail by Explorer 33, *J. Geophys. Res.*, *73*, 907–930.
Behannon, K. (1970), Geometry of the geomagnetic tail, *J. Geophys. Res.*, *75*(4), 743–753, doi:10.1029/JA075i004p00743.
Berchem, J., J. Raeder, M. Ashour-Abdalla, L. A. Frank, W. R. Paterson, K. L. Ackerson, S. Kokubun, T. Yamamoto, and R. P. Lepping (1998), The distant tail at 200 R_E: Comparison between Geotail observations and the results from a global magnetohydrodynamic simulation, *J. Geophys. Res.*, *103*(A5), 9121–9141, doi:10.1029/97JA02926.
Brecht, S., J. Lyon, J. Fedder, and K. Hain (1981), A simulation study of east-west IMF effects on the magnetosphere, *Geophys. Res. Lett.*, *8*, 397–400.
Colella, P., and P. R. Woodward (1984), The piecewise parabolic method (PPM) for gas-dynamical simulations, *J. Comput. Phys.*, *54*(1), 174–201.
Cowley, S. W. H. (1981), Magnetospheric asymmetries associated with the y-component of the IMF, *Planet. Space Sci.*, *29*, 79–96, doi:10.1016/0032-0633(81)90141-0.
Dai, W., and P. R. Woodward (1995), A simple Riemann solver and high-order Godunov schemes for hyperbolic systems of conservation laws, *J. Comput. Phys.*, *121*, 51–65.
Fairfield, D. H. (1971), Average and unusual locations of the Earth's magnetopause and bow shock, *J. Geophys. Res.*, *76*(28), 6700–6716, doi:10.1029/JA076i028p06700.
Fairfield, D. H. (1979), On the average configuration of the geomagnetic tail, *J. Geophys. Res.*, *84*(A5), 1950–1958, doi:10.1029/JA084iA05p01950.
Godunov, S. K. (1959), A difference method for numerical calculation of discontinuous solutions of the equations of hydrodynamics, *Math. Sbornik*, *47*, 271–306.
Hasegawa, H., K. Maezawa, T. Mukai, and Y. Saito (2002a), Plasma entry across the distant tail magnetopause 1. Global properties and IMF dependence, *J. Geophys. Res.*, *107*, A51063, doi:10.1029/2001JA900139.
Hasegawa, H., K. Maezawa, T. Mukai, and Y. Saito (2002b), Plasma entry across the distant tail magnetopause 2. Comparison between MHD theory and observation, *J. Geophys. Res.*, *107*, A51063, doi:10.1029/2001JA900138.
Hu, Y. Q., et al. (2005), Oscillation of quasi-steady Earth's magnetosphere, *Chin. Phys. Lett.*, *22*(10), 2723–2726.
Hu, Y. Q., X. C. Guo, and C. Wang (2007), On the ionospheric and reconnection potentials of the earth: Results from global MHD simulations, *J. Geophys. Res.*, *112*, A07215, doi:10.1029/2006JA012145.

Hu, Y. Q., Z. Peng, C. Wang, and J. R. Kan (2009), Magnetic merging line and reconnection voltage versus IMF clock angle: Results from global MHD simulations, *J. Geophys. Res.*, *114*, A08220, doi:10.1029/2009JA014118.

Kawano, H., S. M. Petrinec, C. T. Russell, and T. Higuchi (1999), Magnetopause shape determinations from measured position and estimated flaring angle, *J. Geophys. Res.*, *104*(A1), 247–261.

Kaymaz, Z., G. L. Siscoe, J. G. Luhmann, R. P. Lepping, and C. T. Russell (1994), Interplanetary magnetic field control of magnetotail magnetic field geometry: IMP 8 observations, *J. Geophys. Res.*, *99*, 11,113-11,126.

Kaymaz, Z., G. L. Siscoe, J. G. Luhmann, J. A. Fedder, and J. G. Lyon (1995), Interplanetary magnetic field control of magnetotail field: IMP 8 data and MHD model compared, *J. Geophys. Res.*, *100*(A9), 17,163–17,172, doi:10.1029/95JA00593.

Lavraud, B., and J. E. Borovsky (2008), Altered solar wind-magnetosphere interaction at low Mach numbers: Coronal mass ejections, *J. Geophys. Res.*, *113*, A00B08, doi:10.1029/2008JA013192.

Liu, Z.-Q., J. Y. Lu, K. Kabin, Y. F. Yang, M. X. Zhao, and X. Cao (2012), Dipole tilt control of the magnetopause for southward IMF from global magnetohydrodynamic simulations, *J. Geophys. Res.*, *117*, A07207, doi:10.1029/2011JA017441.

Lu, J. Y., Z.-Q. Liu, K. Kabin, M. X. Zhao, D. D. Liu, Q. Zhou, and Y. Xiao (2011), Three dimensional shape of the magnetopause: Global MHD results, *J. Geophys. Res.*, *116*, A09237, doi:10.1029/2010JA016418.

Lu, J. Y., Z.-Q. Liu, K. Kabin, H. Jing, M. X. Zhao, and Y. Wang (2013), The IMF dependence of the magnetopause from global MHD simulations, *J. Geophys. Res. Space Physics*, *118*, 3113–3125, doi:10.1002/jgra.50324.

Lyon, J. G., J. A. Fedder, and C. M. Mobarry (2004), The Lyon-Fedder-Mobarry (LFM) global MHD magnetospheric simulation code, *J. Atmos. Sol. Terr. Phys.*, *66*, 1333–1350.

Němeček, Z., J. Šafránková, A. Koval, J. Merka, and L. Prech (2011), MHD analysis of propagation of an interplanetary shock across magnetospheric boundaries, *J. Atmos. Sol. Terr. Phys.*, *73*(1), 20–29.

Owen, C. J., J. A. Slavin, I. G. Richardson, N. Murphy, and R. J. Hynds (1995), Average motion, structure and orientation of the distant magnetotail determined from remote sensing of the edge of the plasma sheet boundary layer with $E > 35$ keV ions, *J. Geophys. Res.*, *100*(A1), 185–204, doi:10.1029/94JA02417.

Palmroth, M., T. I. Pulkkinen, P. Janhunen, and C.-C. Wu (2003), Stormtime energy transfer in global MHD simulation, *J. Geophys. Res.*, *108*(A1), 1048, doi:10.1029/2002JA009446.

Park, K. S., T. Ogino, and R. J. Walker (2006), On the importance of antiparallel reconnection when the dipole tilt and IMF B_y are nonzero, *J. Geophys. Res.*, *111*, A05202, doi:10.1029/2004JA010972.

Petrinec, S. M., and C. T. Russell (1996), Near-Earth magnetotail shape and size as determined from the magnetopause flaring angle, *J. Geophys. Res.*, *101*(A1), 137–152.

Scarf, F. L., L. A. Frank, and R. P. Lepping (1977), Magnetosphere boundary observations along the Imp 7 orbit, 1. Boundary locations and wave level variations, *J. Geophys. Res.*, *82*(32), 5171–5180, doi:10.1029/JA082i032p05171.

Shue, J.-H., J. K. Chao, H. C. Fu, C. T. Russell, P. Song, K. K. Khurana, and H. J. Singer (1997), A new functional form to study the solar wind control of the magnetopause size and shape, *J. Geophys. Res.*, *102*(A5), 9497–9511.

Sibeck, D. G., J. A. Slavin, E. J. Smith, and B. T. Tsurutani (1986), Twisting of the geomagnetic tail, in *Solar Wind-Magnetosphere Coupling*, edited by Y. Kamide, and J. A. Slavin, pp. 731–738, Terra Sci., Tokyo.

Sibeck, D. G., R. E. Lopez, and E. C. Roelof (1991), Solar wind control of the magnetopause shape, location, and motion, *J. Geophys. Res.*, *96*(A4), 5489–5495.

Tsyganenko, N. A., S. B. P. Karlsson, S. Kokubun, T. Yamamoto, A. J. Lazarus, K. W. Ogilvie, C. T. Russell, and J. A. Slavin (1998), Global configuration of the magnetotail current sheet as derived from Geotail, Wind, IMP 8 and ISEE 1/2 data, *J. Geophys. Res.*, *103*(A4), 6827–6841, doi:10.1029/97JA03621.

Villante, U. (1976), Neutral sheet observations at 1000 R_E, *J. Geophys. Res.*, *81*(1), 212–215, doi:10.1029/JA081i001p00212.

Walker, R. J., R. L. Richard, T. Ogino, and M. Ashour-Abdalla (1999), The response of the magnetotail to changes in the IMF orientation: The magnetotail's long memory, *Phys. Chem. Earth*, *24*(1-3), 221–227.